Supporting Information

The Conductance Interplay in Ion Concentration Polarization Across 1D Nanochannels: The Microchannel Surface Shunt and the Nanochannel Conductance

Zisun Ahmed,[a,#] *Yang Bu*,[b,#] *and Levent Yobas*[a,b,*]

[a]Department of Chemical and Biological Engineering,

[b]Department of Electronic and Computer Engineering,

The Hong Kong University of Science and Technology,

Clear Water Bay, Hong Kong SAR, China

[#]Equal contribution

[*]E-mail: eelyobas@ust.hk

Table of Contents:

Simulations. We have adopted the 2D computational model developed by Daiguci et al.[1] as it has been proven on the problems with a known analytical solution. The model featured a 30 nm channel 5 μm long bridging 1 μm × 1 μm reservoirs. However, it did not take into account surface charge on the reservoir walls, thereby assuming an infinitely large R_{SC}. Here, we considered surface charge on the walls of the reservoirs as well as of the nanochannel and solved the model for a 70 nm channel with two distinct lengths (500 nm and 5 μm).

We first obtained ϕ, the electric potential, and n_i, the number density of ions of species i, by solving the Poisson−Nernst−Planck (PNP) equation system for the 2D computational domain:

$$\nabla^2\phi = -\frac{1}{\varepsilon_0\varepsilon}\sum_i z_i e n_i \tag{S-1}$$

and

$$\boldsymbol{J}_i = -D_i\left(\nabla n_i + \frac{z_i e n_i}{kT}\nabla\phi\right) \tag{S-2}$$

where ε is the dielectric constant of aqueous solution, ε_0 the permittivity of free space, k Boltzmann constant, and T temperature in Kelvin whereas $z_i e$, $\boldsymbol{J}_i$, and D_i, are the electric charge, the flux vector, and the diffusion coefficient of ions of species i, respectively. The del operator ∇ signifies the spatial vector gradient.

The steady-state solution $\boldsymbol{J}_i$ must satisfy the continuity equation, $\nabla \cdot \boldsymbol{J}_i = 0$, as well as the boundary conditions at the walls: (1) $\boldsymbol{J}_i = 0$, i.e., no flux, and (2) the potential gradient:

$$\nabla\phi = -\frac{\sigma}{\varepsilon_0\varepsilon} \tag{S-3}$$

where σ is the surface charge density.

The resulting electric current due to the applied bias is given by:

$$I = z_i e \int \sum_i \boldsymbol{J}_i \, dS \tag{S-4}$$

where S is the channel cross-sectional area, πr^2 with r being the nanochannel radius.

Figure S-1 schematically describes the 2D model geometry and the mesh distribution simulated. A coarse mesh was applied in domain 1, away from the nanochannel, while a progressively finer mesh was used in domain 2, nearer to the nanochannel opening to accurately capture its field focusing effect. Yet a finest mesh was chosen in domain 3, the nanochannel. The maximum element size was 200, 10, and 1 nm in respective domains. In domains 1 and 2, near the channel boundaries, a multilayer rectangular grid was used with a layer-to-layer spacing progressively finer down to 1 nm to resolve the influence of the surface charge of the walls. The overall mesh contained 1.8 $\times 10^6$ elements and produced results comparable to those obtained with a finer mesh (12.5 $\times$ 10^6 elements), confirming the mesh independency.

In simulations, the ion concentration levels at the boundaries anode and cathode were set to the reservoir levels. For the background electrolyte, an aqueous solution of potassium chloride (KCl), a symmetric electrolyte, i.e., $z_+ = -z_- = 1$, was assumed with the ion diffusion coefficients at $D_{\mathrm{K}^+} = 1.96\times10^{-9}$ m^2/s and $D_{\mathrm{Cl}^-} = 2.03\times10^{-9}$ m^2/s. The model was solved for an electric potential sweep from 0 to 10 V with step increments of 1 V and the solution for each bias provided the initial condition for the subsequent computation. For each bias, the electric current value was obtained from eq (S-4).

Device fabrication. The process is described through major fabrication steps illustrated in Figure S-2.[2,3] Briefly, advanced oxide etch (AOE) was applied to create trenches 70 μm long and 2 μm wide and deep in a low temperature oxide (LTO) layer 3 μm thick placed through chemical vapor deposition (CVD). Underneath the LTO layer, an additional oxide layer was thermally grown 3 μm thick serving as a further dielectric insulation on silicon. The trenches subsequently received a deposition of a low-stress silicon nitride film 100 nm thick as a diffusion barrier and then of a phosphosilicate glass (PSG) 6 μm thick as a structural layer. This led to a self-enclosed triangular conduit acting as the nanochannel precursor within each

trench owing to the non-conformal step coverage profile of the PSG layer. The conduits were then transformed into tubular structures 500 nm in diameter through PSG reflow during annealing at 1050 °C for 10 min. The diameter was further scaled to 70 nm during the subsequent rapid thermal annealing steps. A final step of UV lithography followed by AOE was applied to open up the nanochannel ends and to structure microchannels 50 μm wide and 5 μm deep. The microchannels were enclosed from above with a slab of silicone elastomer polydimethlysiloxane (PDMS) featuring inlet/outlet holes and secured in place after oxygen-plasma surface activation (30 W, 4 min; Harrick Plasma). The PDMS slab was further secured on the device by a custom-made mechanical clamp.

Movies. In the movies, the cursor (dashed red line) is shown tracing the measured $I-V$ curve obtained from a device at a concurrent speed with the frames of a fluorescent image sequence captured at 2 s intervals from the anodic microchannel. The microchannel contains negatively charged fluorescent particle suspension in KCl solution. The particles leave a dark region as they are repelled from the depletion zone being initiated and developed by the nanochannel(s) subjected to a linear bias sweep at an increment of 0.25 V every 30 s.

Movie S-1. corresponds to Figure 4b (single nanochannel; 1 mM KCl).

Movie S-2. corresponds to Figure 6a (nanochannel array $N = 18$; $s = 4$ μm; 1 mM KCl).

Movie S-3. corresponds to Figure 6b (nanochannel array $N = 18$; $s = 4$ μm; 10 mM KCl).

SUPPORTING FIGURES

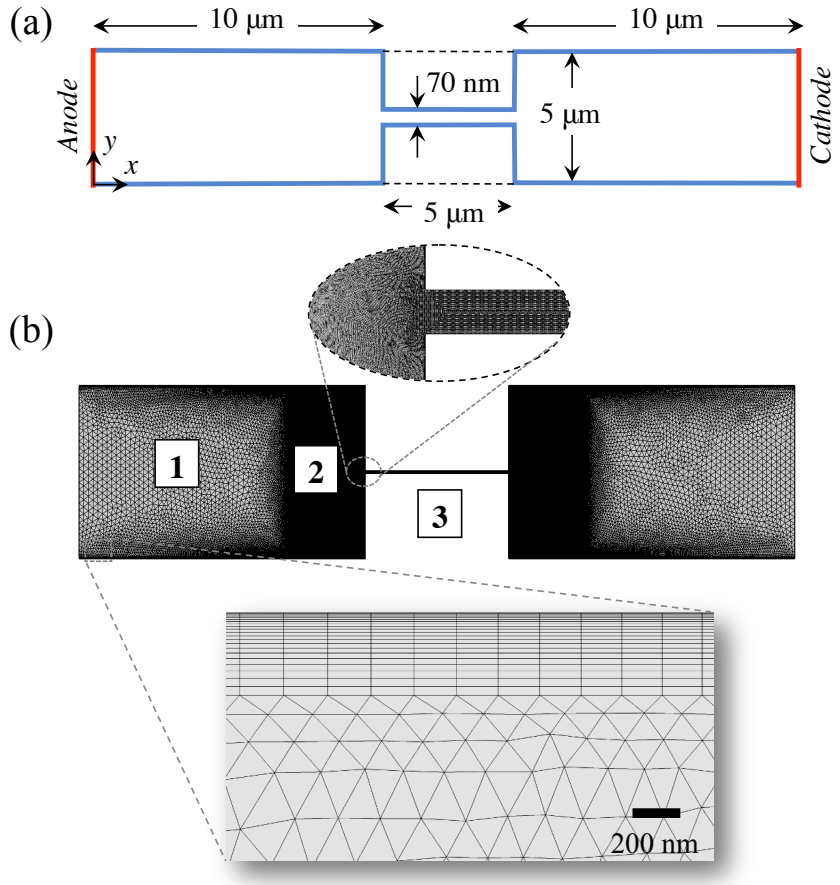

Figure S-1. (a) Schematic description of the 2D model geometry simulated (not drawn to scale). A constant surface charge density was applied to all the boundaries except for the anode and cathode. For comparison, the simulations included deviations from the model in: (1) the surface charge density kept being exclusive to the nanochannel; (2) the nanochannel kept at a length of 500 nm. (b) Typical distribution of mesh elements. Insets: microchannel-nanochannel junction (above) and near the channel boundary (below).

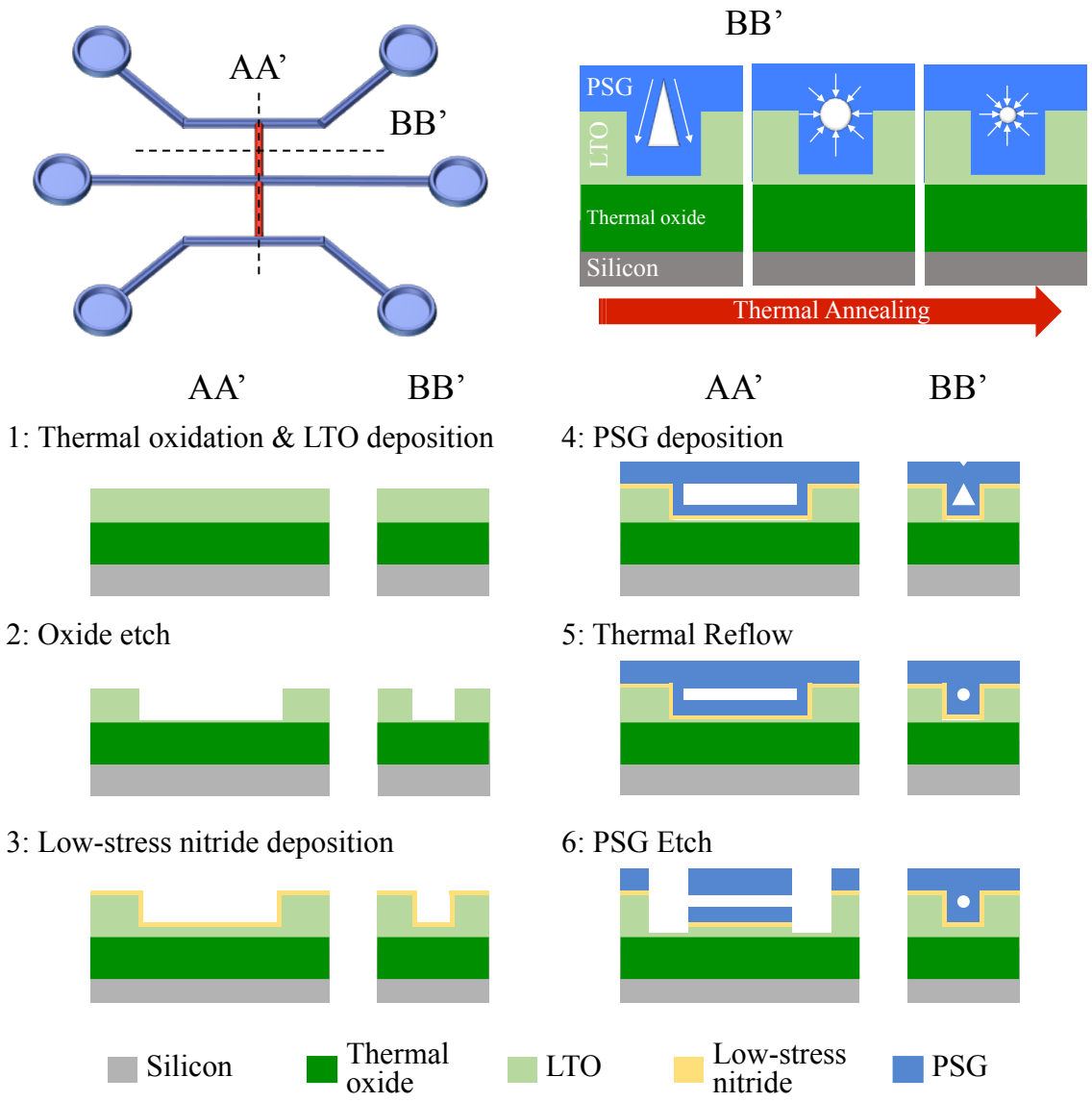

Figure S-2. Device layout and device cutaway diagrams along the dashed lines AA’ and BB’. Above: thermal reflow process illustrated for a self-enclosed channel in phosphosilicate glass (PSG) involving a shape transformation into a tubular geometry and then further scaling into a nanochannel (shrinking). Below: major fabrication steps include (1) thermal oxidation and low temperature oxide (LTO) deposition; (2) oxide etch; (3) low-stress nitride deposition; (4) phosphosilicate glass (PSG) deposition; (5) thermal reflow; and (6) PSG etch.

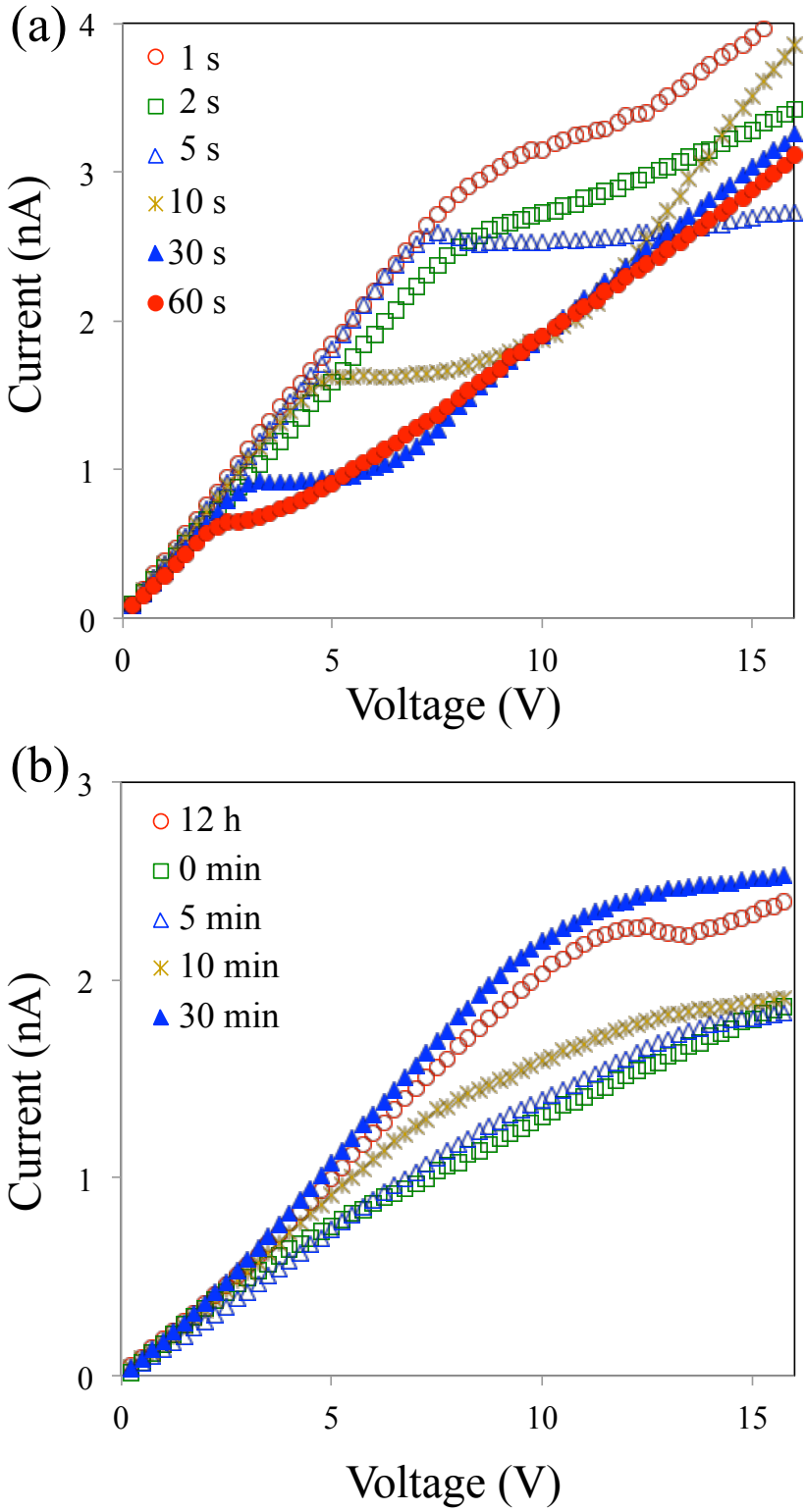

Figure S-3. Nanochannel array ($I - V$) characteristics dependence on (a) the sweep rate and (b) the rest period (legends) shown for KCl ionic strength of (a) 1 mM and (b) 100 μM. The arrays feature 18 nanochannels at an interchannel spacing of 4 μm.

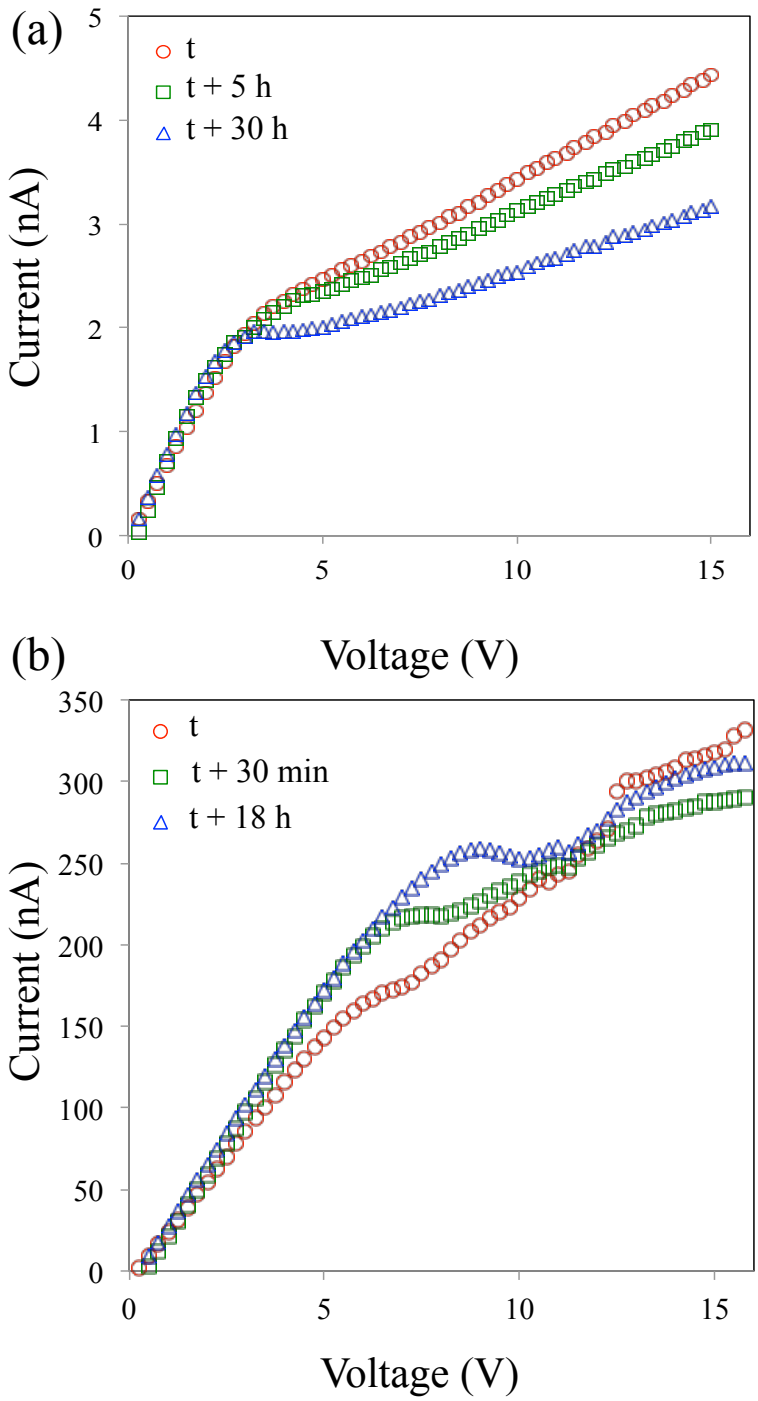

Figure S-4. Nanochannel array ($I-V$) characteristics dependence on time for KCl ionic strength of (a) 1 mM and (b) 200 mM. The arrays feature 18 nanochannels at an interchannel spacing of 4 μm.

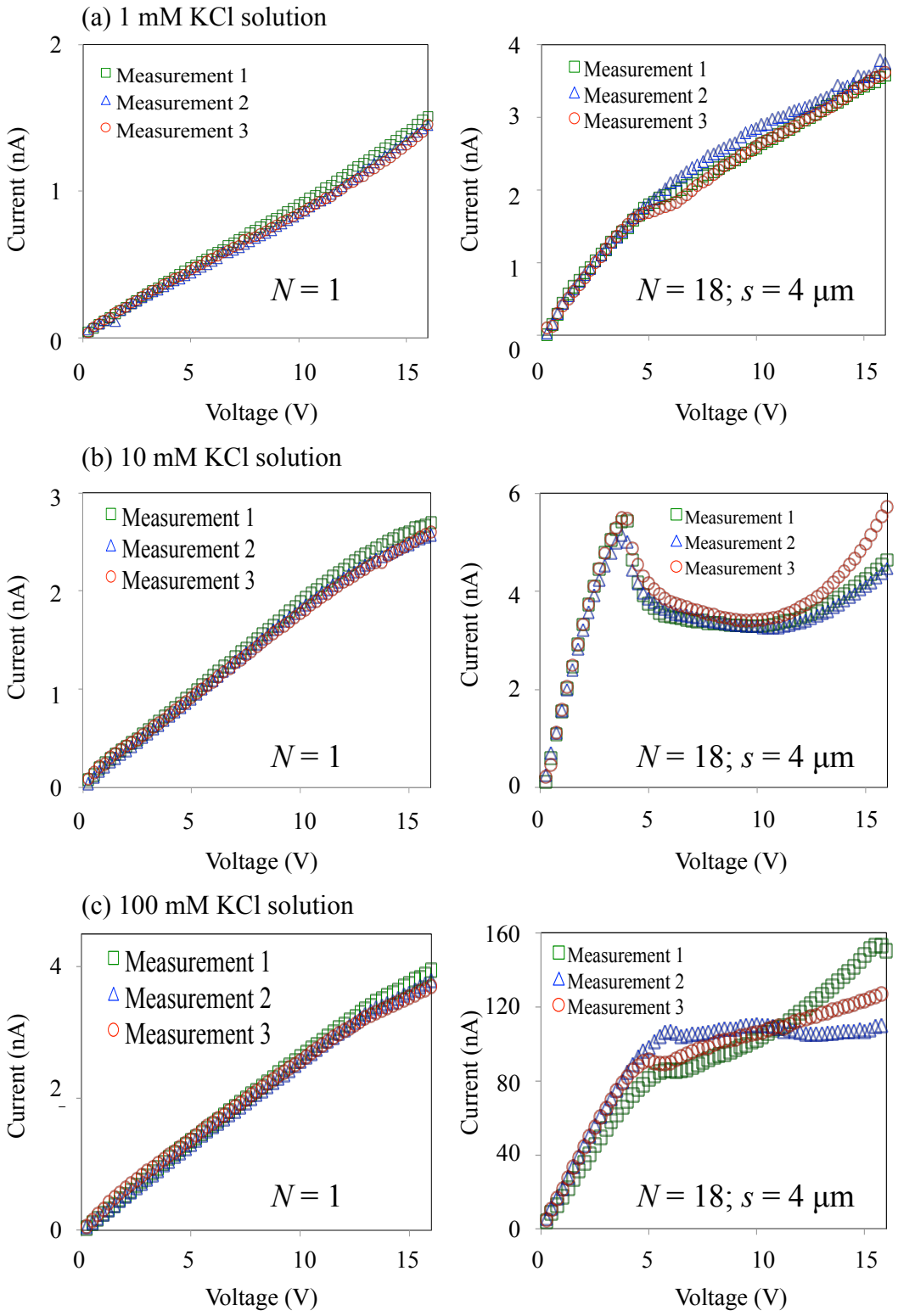

Figure S-5. Plots of $I-V$ measurements. Each plot shows three replicates from a specific device featuring a single nanochannel ($N = 1$) or a nanochannel array ($N = 18$; $s = 4$ μm) for KCl ionic strength of (a) 1 mM (b) 10 mM and (c) 100 mM.

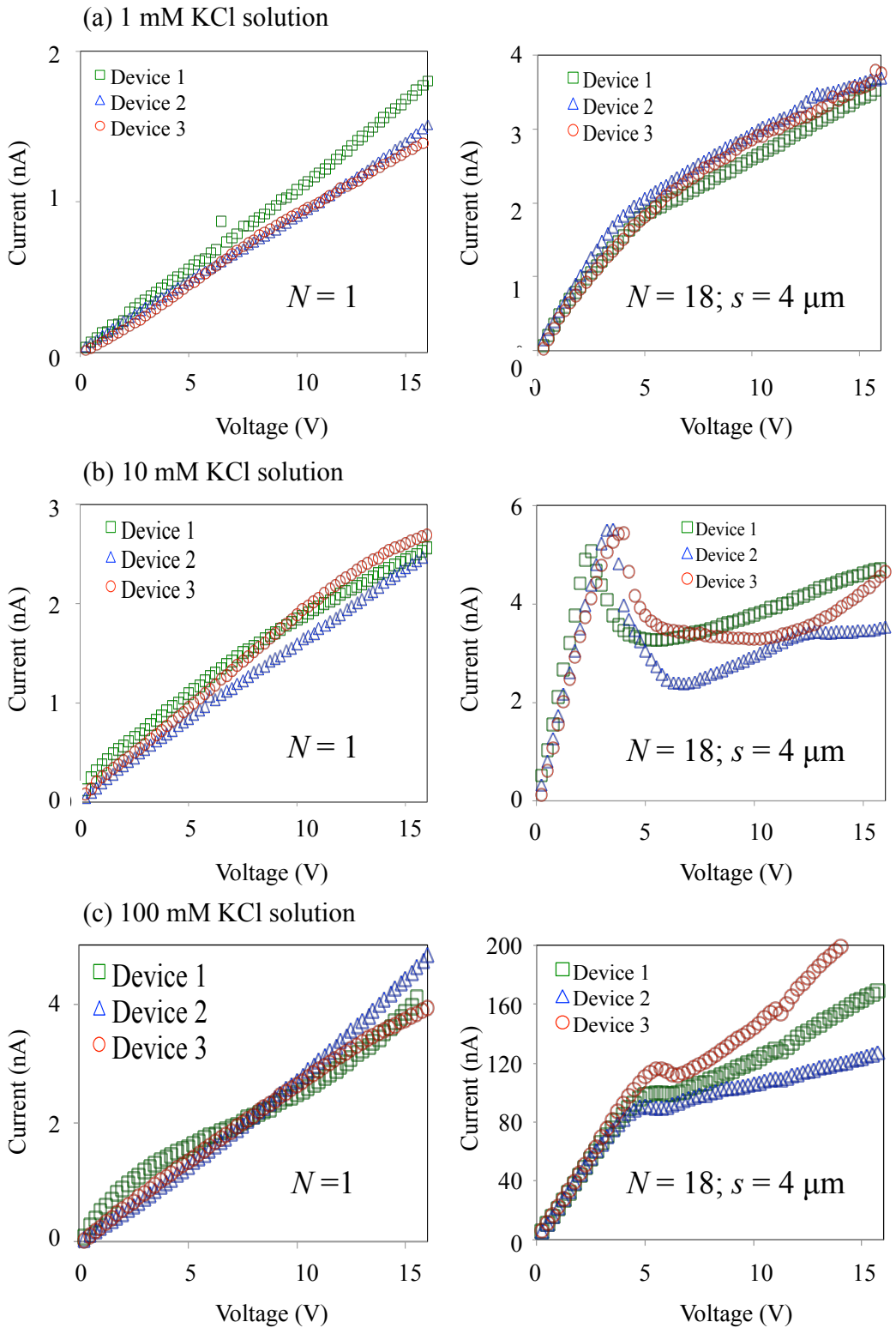

Figure S-6. Plots of $I-V$ measurements. Each plot shows three independent measurements with each measurement from a distinct device featuring a single nanochannel ($N = 1$) or a nanochannel array ($N = 18$; $s = 4$ μm) for KCl ionic strength of (a) 1 mM (b) 10 mM and (c) 100 mM.

REFERENCES

(1) Daiguji, H.; Yang, P.; Majumdar, A. Ion Transport in Nanofluidic Channels. *Nano Lett.* **2004**, *4* (1), 137–142.

(2) Cao, Z.; Yobas, L. Gel-Free Electrophoresis of DNA and Proteins on Chips Featuring a 70 Nm Capillary-Well Motif. *ACS Nano* **2015**, *9* (1), 427–435.

(3) Duan, L.; Cao, Z.; Yobas, L. Continuous-Flow Electrophoresis of DNA and Proteins in a Two-Dimensional Capillary-Well Sieve. *Anal. Chem.* **2017**, *89* (18), 10022–10028.